Food Chemistry 470 (2025) 142619

Contents lists available at ScienceDirect

Food Chemistry

journal homepage: www.elsevier.com/locate/foodchem

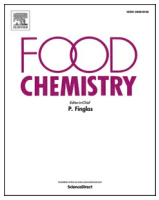

Application of chemometrics based on digital image analysis for simultaneous determination of tartrazine and sunset yellow in food samples

Seyyedeh Fatemeh Hosseini [a], Tahereh Heidari [a,*], Ameneh Zendegi-Shiraz [b], Majid Ameri [c]

[a] Department of Chemistry, Faculty of Sciences, Ferdowsi University of Mashhad, Mashhad, Iran
[b] Department of Chemistry, Science and Research Branch, Islamic Azad University, Tehran, Iran
[c] Department of chemistry, University of Science and Technology, Tehran, Iran

ARTICLE INFO

Keywords:
Food dyes
PLS
Color channel
Histogram
RGB
HSI
HPLC

ABSTRACT

Azo dyes, such as tartrazine and sunset yellow, are widely used as affordable and stable food colorants. Accurate quantification is crucial in foods for regulatory monitoring to ensure compliance with safety standards and minimize health risks. This study developed a low-cost and eco-friendly method using digital images and chemometrics for the simultaneous determination of these dyes in food samples. The best prediction results were achieved by applying partial least squares regression to RGB + Grayscale+HSI color histograms, with R^2 of 0.9977, 0.9989, RMSEP of 0.21, 0.10 mg/L and REP of 1.6, 1.0 % for tartrazine and sunset yellow, respectively. The method was successfully applied for determination of tartrazine and sunset yellow in soft drink samples, producing results comparable to those obtained from the HPLC method. This innovative approach provides a practical and reliable alternative for monitoring the dye concentrations, supporting both food manufacturers and health authorities in ensuring compliance with safety standards.

1. Introduction

Artificial food dyes, such as tartrazine (Tar) and sunset yellow (SY), are common azo anionic dyes widely used to enhance the appearance and consumer appeal of various food products (Do Nascimento et al., 2020; Rozamliana et al., 2024; Zhang et al., 2024). Tartrazine, known for providing a bright yellow hue, is the second most commonly used food dye globally. It is especially prevalent in products such as soft drinks, juices, candies, and sauces (Wu & Lee, 2020). Additionally, sunset yellow, which is the third most widely used food dye, is frequently found in sweets, jams, and fermented beverages (Banc et al., 2024; Darabi & Shabani-Nooshabadi, 2021).

Despite their widespread use, overconsumption of these dyes may lead to health issues, particularly in sensitive individuals, causing effects such as allergies, migraines, hyperactivity, and other health concerns (Bakhnooh & Arvand, 2024; Chaudhari et al., 2024; Fan et al., 2024; Wang et al., 2024; Zhang et al., 2025).

For instance, regulations in the European Union (EU) limit the concentrations of tartrazine and sunset yellow in non-alcoholic soft drinks to 100 mg/L and 50 mg/L, respectively, with a total limit of 100 mg/L when used together. Likewise, in the United States (US), the acceptable daily intake (ADI) for tartrazine is 7.5 mg/kg body weight per day, and for sunset yellow, it is 4 mg/kg body weight per day (EFSA Panel on Food Additives and Nutrient Sources Added to Food, 2009a; EFSA Panel on Food Additives and Nutrient Sources Added to Food, 2009b; EFSA Panel on Food Additives and Nutrient Sources added to Food (ANS), 2014; Rovina et al., 2017; Park et al., 2024; Amchova et al., 2024). To ensure compliance with safety standards, reliable methods for the simultaneous determination of these dyes are crucial (Darabi & Shabani-Nooshabadi, 2021). High-performance liquid chromatography (HPLC) coupled with UV–Vis detection is a standard method for precise dye quantification, known for its high sensitivity and reliability (Agbokponto et al., 2022). However, it is also associated with high costs, the use of toxic solvents, and the need for specialized training and equipment, which suffer environmental, economic, and personal challenges. These obstacles can limit the accessibility of this method. Other techniques, such as electrochemical analysis (Taei et al., 2020), spectrophotometry (Asadollahi et al., 2022), and capillary electrophoresis (Flores-Aguilar et al., 2019), have been used for the simultaneous determination of Tar and SY, but each presents its own limitations in terms of equipment costs, preparation time, and the need for skilled operators (Ostad & Heidari, 2020). Recent advancements in digital imaging and chemometrics offer a promising alternative for dye analysis (Ostad & Heidari, 2020). With the availability of digital devices such as

* Corresponding author.
E-mail address: taherehheidari@um.ac.ir (T. Heidari).

https://doi.org/10.1016/j.foodchem.2024.142619
Received 22 August 2024; Received in revised form 10 December 2024; Accepted 21 December 2024
Available online 24 December 2024

smartphones and scanners, digital imaging-based colorimetric analysis method has emerged as a user-friendly, accessible, and non-destructive method suitable for both qualitative and quantitative analysis in food assessment (Choi et al., 2018; Guedes & Pereira, 2019; Santos et al., 2020).

Commercial software such as Adobe Photoshop and MATLAB are widely used for image processing and analysis; however, their high cost and complex training requirements make them less accessible for small labs and independent researchers (Ahmed, 2013; Riedel et al., 2023; Timothy & Forlano, 2019). Photoshop, for example, offers extensive capabilities for digital art creation, drawing, and editing. Though, free alternatives like ImageJ provide a more accessible option, available both as an online applet and a downloadable application, making it a practical solution for those seeking cost-effective tools (Harris-Love et al., 2016; Lin et al., 2023; Timothy & Forlano, 2019).

A digital image is made up of many pixels, each containing three color components—red, green, and blue—known as the RGB color model. Other color models, such as HSI and HSV, are also used (Fiedoruk-Pogrebniak, 2024). Once the image is converted into a color model and numerical data is generated, chemometrics methods can be applied to extract useful information (Ribeiro et al., 2019). Color histograms, which show the distribution of pixel color frequencies, can also serve as input for multivariate analysis.

Digital image analysis combined with chemometrics is a powerful tool for both qualitative and quantitative analysis of food products, including milk, coffee, olive oil, saffron, grape juice, and chicken burgers (Beltrame et al., 2019; De Araújo et al., 2021; De Sousa Fernandes et al., 2019; Dos Santos Pereira et al., 2022; Song et al., 2020). Previous studies have also used chemometrics methods to determine dyes like tartrazine (Vidal et al., 2018) and sunset yellow (Botelho et al., 2014) in foods, with successful applications in candies and soft drinks. Partial least square (PLS) regression is the most popular tool in chemometrics for developing calibration models. PLS algorithm has been successfully combined with spectroscopic (Brereton, 2003, 2007, 2018; Kumar, 2021) and recently digital image analysis (Botelho et al., 2017; Qashqai & Heidari, 2023; Costa et al., 2020; De Sousa Fernandes et al., 2019, De Sousa Fernandes et al., 2019).

This study proposes a digital imaging-based multivariate calibration method for the simultaneous determination of Tar and SY, focusing on three image analysis approaches: color channel analysis, effective color channel analysis, and a color histogram-based analytical system. This innovative method was applied to 10 soft drink samples, and results were validated against the HPLC method to assess its accuracy and applicability in real samples.

2. Materials and methods

2.1. Chemicals

HPLC grade acetonitrile and methanol were purchased from Merck (Merck KGaA, Darmstadt, Germany). Tartrazine and sunset yellow were obtained from Sigma Aldrich (St. Louis, MO, USA). All experiments were carried out at room temperature, using materials of analytical purity grade without further purification. All solutions used in the experiments were prepared with deionized water.

2.2. Instrument and software

Image capturing was performed using a Canon Lide 120 scanner (Canon Inc., Tokyo, Japan), and images were saved in JPEG format. The SPL microplates (The SPL Life Sciences, Pocheon, Korea) were used for sample placement within the scanner. To keep away from external light, all images were taken in a dark environment. Each sample was captured three times to ensure consistent image quality. The region of interest (ROI) was manually selected using the elliptical marquee tool in Adobe Photoshop CS5 2018 (Adobe Systems, Inc., San Jose, CA, USA) (Harris-Love et al., 2016; Hua et al., 2020). The ROI selection focused on areas with distinguishable colors corresponding to the dyes, excluding background noise. This manual selection method, while direct and straightforward, may be subject to personal bias (Jia et al., 2020; Vidal & Amigo, 2012). To reduce this, all selections were reviewed by a trained individual, minimizing the potential impact of personal preferences. Adobe Photoshop provides various selection tools that facilitate the effective identification and isolation of the ROI for subsequent analysis (Wang et al., 2015).

Adobe Photoshop CS5 (2018) software was utilized to extract color channels from digital images. The extracted channels included Red (R), Green (G), and Blue (B) from the RGB model; Cyan (C), Magenta (M), Yellow (Y), and Black (K) from the CMYK model; grayscale (g); and Hue (H), Saturation (S), and Intensity (I) from the HSI model (Grudpan et al., 2015). MATLAB R2013a (The MathWorks, Natick, USA) software was applied to analyze the data, including color channels and color histograms. In order to convert digital image into histogram, free MATLAB "Imagens_gui" interface was used (Diniz, 2020). Color histograms were involving RGB, grayscale, and HSI. Average histograms were taken as input data to do calculations. Partial least squares regression (PLS) was done by MVC1_GUI toolbox in MATLAB (Amsaraj & Mutturi, 2024).

2.3. Univariate calibration method

Initially, digital images were captured for individual calibration solutions of Tar and SY. These images were converted into RGB and CMYK color models. The calibration curves were constructed by plotting each color channel against concentrations of Tar and SY. The best color channel was selected based on its linear relationship with the concentration of Tar and SY.

2.4. Multivariate calibration method

To simultaneously determine Tar and SY, color channels, effective color channels, and color histograms were applied as input data to construct PLS regression model.

The color channels including red, green, blue, cyan, magenta, yellow, black, grayscale and hue, saturation and intensity were evaluated and effective color channels were selected.

Effective color channels were identified based on their linear relationship with dye concentrations. Calibration plots were constructed for each color channel by plotting dye concentrations against the corresponding intensity values. Channels with the highest correlation coefficients ($R^2 \geq 0.99$) were selected as effective channels, ensuring the reliability and accuracy of these channels for quantifying dye concentrations in the samples. After determining the effective color channels, the contribution of the remaining color channels was evaluated using the forward feature selection method. Forward feature selection identifies the most significant attributes while eliminating irrelevant ones. In this approach, features are added one by one, and the model's accuracy is assessed at each step to see if it improves with the addition of the new feature. If accuracy does not increase or remains unchanged, those features are considered unnecessary and excluded. This process ensures that only essential features are retained in the final model. (Jia et al., 2020; Nakanishi et al., 2024; Rahma et al., 2023).

Additionally, PLS-assisted color histogram-based analytical systems was employed. Various color histogram combinations—such as Grayscale, RGB, HSI, Grayscale + RGB, Grayscale + HSI, RGB + HSI, and RGB + Grayscale + HSI—were assessed to build the regression model.

Twenty standard solutions were carefully prepared, containing a mixture of Tar and SY within linear ranges of 2–29 mg/L and 3–22 mg/L, respectively. Ten samples were randomly selected as calibration samples, while the remaining ten were used as prediction samples to evaluate the performance of the proposed method. The performance of the model in the calibration set was expressed by the coefficient of correlation for cross-validation (R^2_{CV}) and the root mean square error of cross-

Table 1
Figures of merit for determination of Tar and SY using scanner-based colorimetric method (yellow color channel) and HPLC.

Method	Analyte	Linear range (mg/L)	Equation	R^2	LOD[c] (mg/L)	LOQ[d] (mg/L)	RSD[e] (%)
Scanner-based colorimetry	Tar[a]	2–29	Y = 7.3753× + 0.0146	0.9998	0.6	2	0.6
	SY[b]	3–22	Y = 9.5862× + 0.3693	0.9988	0.9	3	1.2
HPLC	Tar	0.07–200	Y = 28.67× + 16.408	0.9995	0.02	0.07	2.0
	SY	0.07–200	Y = 30.654× + 2.9899	1	0.02	0.07	0.7

[a] Tartrazine
[b] Sunset yellow
[c] Limit of detection
[d] Limit of quantitation
[e] Relative standard error.

validation (RMSECV). The model's predictive capability was assessed using the coefficient of determination for the prediction (R^2_{Pred}), the root mean square error of prediction (RMSEP), and the relative error of prediction (REP). Additionally, the Elliptical Joint Confidence Region (EJCR) plot in the prediction model was considered to evaluate the model's accuracy and to check for any bias in the results (Fernandes et al., 2023; Qashqai & Heidari, 2023; Ramo et al., 2024).

2.5. Real sample analysis

One batch of 10 different commercially available non-alcoholic soft drink samples was collected from various markets in Iran. The selected drinks consisted of only one type: fruit-flavored, carbonated beverages. Ingredient labels indicated the presence of artificial colors, exclusively sunset yellow, though specific concentrations of this dye were not labeled.

The samples were degassed using an ultrasonic bath for 5 min. All samples, except for sample number 4, showed sunset yellow concentrations exceeding the linear range. To address this, these samples were diluted fivefold to bring their concentrations within acceptable levels. Sample number 4 was already within the linear range and did not require dilution. Deionized water was used as the solvent for the dilutions.

Subsequently, the initial concentrations of Tar and SY were simultaneously determined using the proposed method.

The performance of the proposed method was evaluated using a total of 10 independent replicates (10 samples) and 6 technical replicates.

2.6. Chromatographic analysis

The chromatographic analysis was performed using an Agilent 1100 HPLC system (Agilent Technologies, Santa Clara, CA, USA) equipped with a quaternary pump and a manual injection system with a 20 μL injection loop. A Phenomenex C18 column of 4.6 × 250 mm (Phenomenex Inc., Torrance, CA, USA) was utilized for the separation of the dyes. The mobile phase consisted of acetonitrile and methanol in a ratio of 80:20 (*v*/v), delivered at a flow rate of 1 mL/min. The analysis times were 5.6 min for Tar and 7.7 min for SY, with detection carried out at 445 nm using a UV detector. The column was maintained at room temperature throughout the analysis (Pedjie, 2012).

3. Result and discussion

3.1. Individual calibration of tartrazine and sunset yellow

The linearity of R, G, B, C, M, Y, K, and grayscale color channels was evaluated against the calibration concentrations of Tar and SY, individually. Among these, the yellow channel exhibited the strongest linear relationship with the concentrations. Table 1 compares the figures of merit for the scanner-based colorimetric method using the yellow channel with those obtained by the HPLC method for analysis of Tar and SY.

Table 2
Composition of calibration and prediction sets of Tar and SY for PLS regressions.

Number of samples	Calibration set		Prediction set	
	Tar [a](mg/L)	SY [b](mg/L)	Tar (mg/L)	SY (mg/L)
1	8.5	10	8	14
2	9.5	9.5	9	13
3	10.5	9	10	12.5
4	11	8.5	10.5	11.5
5	11.5	8.5	12	10
6	12	8	13	9
7	12.5	7.5	14	8
8	13	7	15	6.5
9	13.5	6.5	15.5	6
10	14	6	16	6

[a] Tartrazine
[b] Sunset yellow.

3.2. Simultaneous determination of tartrazine and sunset yellow

The first stage in the simultaneous determination of the binary mixture of Tar and SY with the multivariate calibration method involved the construction of the calibration and prediction sets. The composition of the calibration and prediction sets is provided in Table 2. These sets were designed to include a representative range of concentrations to ensure the robustness of the calibration models and the reliability of the predictions. The randomization of sample selection helped to minimize potential systematic errors and validated the applicability of the method across different concentrations.

In this study, Tar and SY were simultaneously determined using the PLS regression method, a robust chemometrics technique that facilitates the analysis of multiple variables simultaneously (Wold et al., 2001). Various input data, including color channels, effective color channels, and color histograms were evaluated.

3.2.1. PLS-assisted color channels -based analytical systems

The analysis involved a comprehensive evaluation of the color channels, including red, green, blue (RGB), cyan, magenta, yellow, black (CMYK), grayscale, as well as hue, saturation, and intensity (HSI) for constructing PLS regression method. The results are summarized in Table 3.

The R^2_{Pred} were found to be 0.9913 for Tar and 0.9931 for SY, indicating a strong predictive capability of the multivariate calibration model.

In Fig. 1(a, c), predicted values are plotted against actual values for both dyes. The random scatter of points around the line suggests that the model's predictions are free from systematic error and are unbiased, which confirms the reliability of the calibration method.

The EJCR region forms an elliptical shape, and it examines whether the theoretically expected values (slope = 1 and intercept = 0) fall within this ellipse. When the ideal point is included in the EJCR, it confirms the accuracy of the methodology (Lozano et al., 2014). Fig. 1(b, d) illustrates the EJCR plots (at 95 % confidence level) for analysis of Tar

Table 3
Results of PLS-assisted color channels for simultaneous determination of Tar and SY.

		Calibration			Prediction		
Color channels	Analyte	LV[c]	R^2_{CV}[d]	RMSECV[e] (mg/L)	R^2_{Pred}[f]	RMSEP[g] (mg/L)	REP[h] (%)
RGB+ CMYK+ grayscale+ HSI	Tar[a]	3	0.2349	0.31	0.9913	0.54	4.3
	SY[b]	3	0.3833	0.30	0.9931	0.43	4.4

R: Red; G: Green; B: Blue; C: Cyan; M: Magenta; Y: Yellow; K: Black; g: grayscale; H: Hue; S: Saturation; I: Intensity.
[a] Tartrazine
[b] Sunset yellow
[c] Latent variable
[d] Coefficient of determination for cross-validation
[e] Root mean square error of cross validation
[f] Coefficient of determination for the prediction
[g] Root mean square error of prediction
[h] Relative error of prediction.

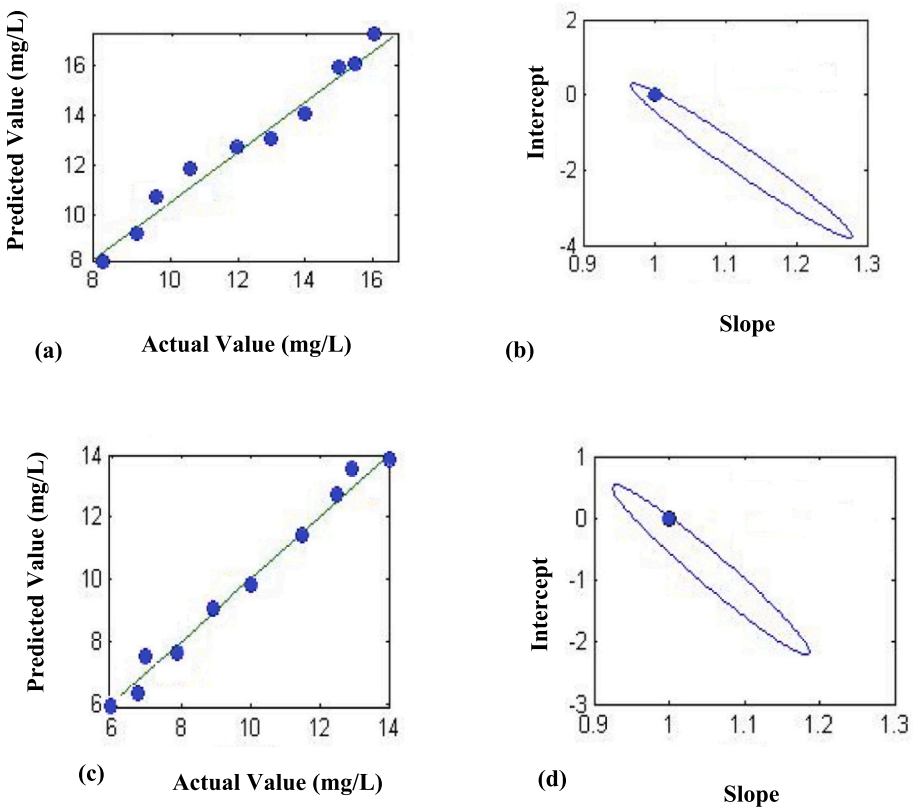

Fig. 1. PLS results and EJCR plots of predicted vs. actual values using the color channels for Tar (a, b) and SY (c, d).

and SY. As seen, they reveal the absence of bias.

The study highlights the potential of digital scanner images as a practical tool for simultaneous determination of the dyes in mixture samples (Botelho et al., 2014).

3.2.2. *PLS-assisted effective color channels -based analytical systems*

In this study, feature selection was applied to identify effective color channels to simplify PLS regression and enhance the model's performance (Canero et al., 2024; Lin et al., 2023). As described in Section 2.4, effective color channels were identified based on the linear relationship between dye concentrations and each color channel using univariate calibration for Tar and SY individually ($R^2 \geq 0.99$). The results indicated that the Green, Blue, Yellow, grayscale, Saturation, and Intensity were the most effective color channels for determining both Tar and SY (Table 4). This targeted approach led to a significant improvement in the R^2_{CV}, which increased to 0.8468 for Tar and 0.8759 for SY. As a result, the RMSECV decreased to 0.14 mg/L for Tar and 0.23 mg/L for SY, highlighting the effectiveness of the model. Additionally, after determining the effective color channels, the contribution of the remaining color channels was evaluated using the forward feature selection method (Table 4). No significant improvement in the performance of PLS for the simultaneous analysis of Tar and SY was observed. As a result, the Green, Blue, Yellow, grayscale, Saturation, and Intensity were considered as the optimal channels for simultaneous determination of Tar and SY in mixture samples using PLS regression.

These enhancements in model performance highlight the critical importance of feature selection in multivariate calibration. Previous studies have similarly demonstrated that selecting relevant features can substantially improve the robustness and predictive accuracy of PLS regression (Amsaraj & Mutturi, 2021 & Amsaraj & Mutturi, 2023).

Fig. 2 illustrates the predicted concentrations of Tar and SY against the actual values. The EJCR plots indicate that reliable results were achieved.

Table 4
Results of PLS-assisted effective color channels for simultaneous determination of Tar and SY.

Selected Color Channels		Calibration			Prediction		
	Analyte	LV[c]	R^2_{CV}[d]	RMSECV[e] (mg/L)	R^2_{Pred}[f]	RMSEP[g] (mg/L)	REP[h] (%)
GBYgSI	Tar [a]	6	0.8468	0.14	0.9938	0.48	3.9
	SY [b]	5	0.8759	0.23	0.9968	0.23	2.4
GBYgSI+ R	Tar	4	0.2190	0.24	0.9922	0.54	4.4
	SY	4	0.2426	0.23	0.9949	0.29	2.9
GBYgSI+C	Tar	5	0.1300	0.29	0.9903	0.58	4.6
	SY	3	0.6690	1.09	0.9921	0.37	3.8
GBYgSI+M	Tar	3	0.3434	0.44	0.9886	0.82	6.6
	SY	3	0.1237	0.42	0.9900	0.92	9.4
GBYgSI+K	Tar	5	0.7609	0.29	0.9931	0.56	4.5
	SY	5	0.1221	0.31	0.9917	0.24	2.4
GBYgSI+H	Tar	4	0.5415	0.32	0.9914	0.53	4.3
	SY	4	0.2200	0.21	0.9944	0.30	3.1

*R: Red; G: Green; B: Blue; C: Cyan; M: Magenta; Y: Yellow; K: Black; g: grayscale; H: Hue; S: Saturation; I: Intensity.
[a] Tartrazine
[b] Sunset yellow
[c] Latent variable
[d] Coefficient of determination for cross-validation
[e] Root mean square error of cross validation
[f] Coefficient of determination for the prediction
[g] Root mean square error of prediction
[h] Relative error of prediction.

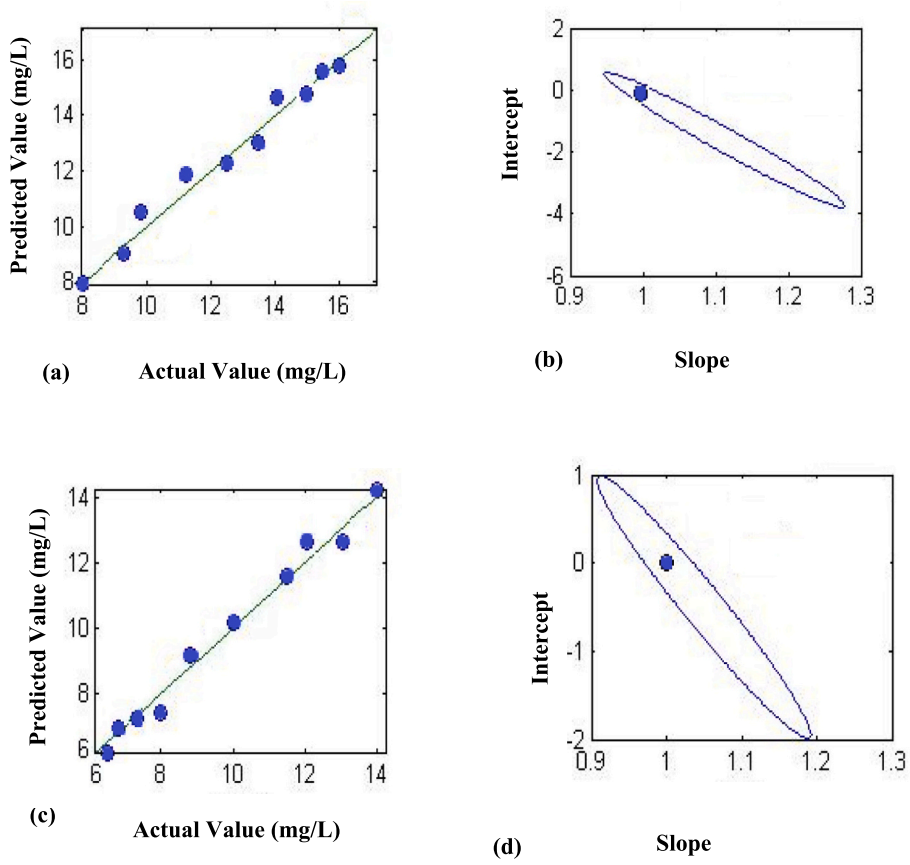

Fig. 2. PLS results and EJCR plots of predicted vs. actual values using effective color channels for Tar (a, b) and SY (c, d).

3.2.3. PLS-assisted color histogram-based analytical systems

In image processing, a color histogram is a quantitative representation of the distribution of color intensities in a digital image (Swain & Ballard, 1991; Zhang et al., 1995).

The color histogram can be built for any kind of color model including RGB, HSI, HSV and gray scale. Pre-processing techniques, such as noise reduction and image segmentation based on pixels or edges, may be applied to the color channels to enhance the quality of the data (Diniz, 2020). However, one of the major advantages of using color histograms is their simplicity; they allow for quick and direct extraction of information without the need for complex pre-processing, enabling data to be analyzed in its original form (De Sousa Fernandes et al., 2019; Reile et al., 2020). The use of color histograms as an analytical signal emerges as a good alternative, because they provide a straightforward

Table 5
Results of PLS-assisted color histogram for simultaneous determination Tar and SY.

Color histogram	Analyte	Calibration			Prediction		
		LV [c]	R^2_{CV} [d]	RMSECV [e] (mg/L)	R^2_{Pred} [f]	RMSEP [g] (mg/L)	REP [h] (%)
Grayscale	Tar [a]	3	0.8643	1.32	0.8928	1.40	11.2
	SY [b]	3	0.8865	1.23	0.9232	1.01	10.4
RGB	Tar	4	0.8812	0.89	0.9229	1.20	9.9
	SY	4	0.9092	0.91	0.9477	1.22	12.5
HSI	Tar	3	0.8901	0.64	0.9377	0.93	7.5
	SY	5	0.9298	0.71	0.9622	1.04	10.7
Grayscale+RGB	Tar	3	0.8955	0.84	0.9346	1.10	9.05
	SY	4	0.9100	2.15	0.9592	1.20	11.9
Grayscale+HSI	Tar	4	0.9023	0.53	0.9469	0.87	6.9
	SY	5	0.9211	1.54	0.9680	1.00	10.3
RGB + HSI	Tar	4	0.9078	0.53	0.9422	0.91	7.2
	SY	5	0.9261	0.36	0.9667	1.00	10.3
RGB + Grayscale+ HSI	Tar	6	0.9572	0.10	0.9977	0.21	1.6
	SY	6	0.9519	0.13	0.9989	0.10	1.0

[a] Tartrazine
[b] Sunset yellow
[c] Latent variable
[d] Coefficient of determination for cross-validation
[e] Root mean square error of cross validation
[f] Coefficient of determination for the prediction
[g] Root mean square error of prediction
[h] Relative error of prediction.

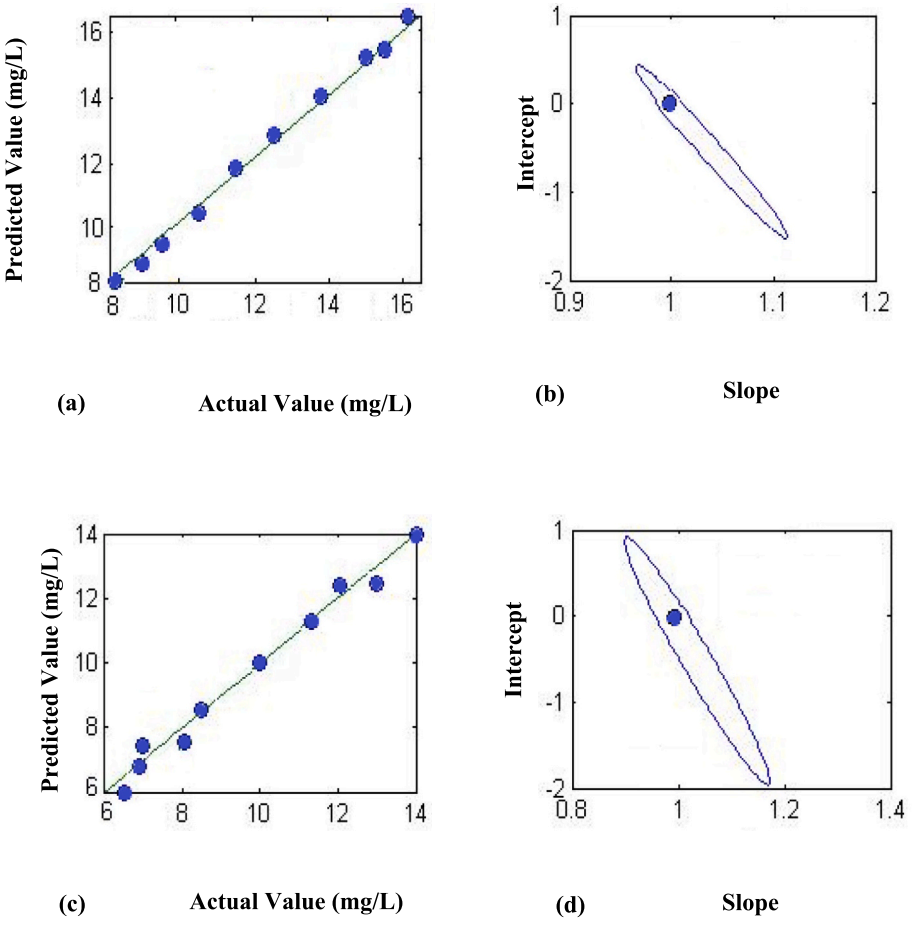

Fig. 3. PLS results and EJCR plot of predicted vs. actual values using RGB + Grayscale + HSI histograms for Tar (a, b) and SY (c, d).

method for rapid acquisition of the analytical information when coupled with multivariate chemometrics methods (Diniz, 2020; De Morais & de Lima, 2015).

Although color histogram analysis provides valuable insights into the distribution of color intensities, interpreting the results can be challenging due to the inherent complexity of frequency distributions (Diniz, 2020; Reile et al., 2020).

In this study, color histograms were generated for Grayscale, RGB,

Table 6
Quantification results of optimal models for simultaneous determination of Tar and SY using PLS-assisted color channels, effective color channels, and color histograms.

		Calibration			Prediction		
Input data	Analyte	LV[c]	R^2_{CV}[d]	RMSECV[e] (mg/L)	R^2_{Pred}[f]	RMSEP[g] (mg/L)	REP[h] (%)
Color channels							
RGB+ CMYK+ grayscale+ HSI	Tar[a]	3	0.2349	0.31	0.9913	0.54	4.3
	SY[b]	3	0.3833	0.30	0.9931	0.43	4.4
Effective color channels							
GBYgSI	Tar	6	0.8468	0.14	0.9938	0.48	3.9
	SY	5	0.8759	0.23	0.9968	0.23	2.4
Color histograms							
RGB + Grayscale + HSI	Tar	6	0.9572	0.10	0.9977	0.21	1.6
	SY	6	0.9519	0.13	0.9989	0.10	1.0

*R: Red; G: Green; B: Blue; C: Cyan; M: Magenta; Y: Yellow; K: Black; g: grayscale; H: Hue; S: Saturation; I: Intensity.
[a] Tartrazine
[b] Sunset yellow
[c] Latent variable
[d] Coefficient of determination for cross-validation
[e] Root mean square error of cross validation
[f] Coefficient of determination for the prediction
[g] Root mean square error of prediction
[h] Relative error of prediction.

Table 7
Simultaneous determination of Tar and SY in soft drinks using PLS-assisted RGB+ Grayscale+ HSI histograms and HPLC.

	PLS-assisted RGB+ Grayscale+ HSI histograms				HPLC				
Sample	Tar[a]		SY[b]		Tar		SY		
	Con. (mg/L)	RSD (%)	Con. (mg/L)	RSD (%)	Con. (mg/L)	RSD (%)	Con. (mg/L)	RSD (%)	t-value[g]
S1	ND[c]	–	30.0[d] ± 0.5[e]	1.6	ND	–	30.37[f] ± 2.1	4.6	0.51
S2	ND	–	33.1 ± 0.9	2.6	0.28 ± 0.01	2.7	33.9 ± 0.4	0.7	1.14
S3	ND	–	21.2 ± 0.3	1.3	0.18 ± 0.01	4.7	21.2 ± 0.7	2.2	0.69
S4	ND	–	12.1 ± 0.2	2.0	ND	–	12.8 ± 0.6	2.7	1.51
S5	ND	–	27.6 ± 0.8	1.7	0.13 ± 0.02	2.8	27.4 ± 0.4	0.8	0.67
S6	ND	–	48.2 ± 0.6	1.2	ND	–	48.39 ± 2.2	2.9	0.27
S7	ND	–	40.2 ± 0.8	1.8	0.191 ± 0.006	2.0	40.5 ± 0.7	1.2	0.49
S8	ND	–	50.8 ± 1.1	2.1	0.166 ± 0.003	4.0	50.96 ± 1.4	1.7	0.26
S9	ND	–	48.5 ± 0.6	1.3	ND	–	48.6 ± 0.6	1.3	0.26
S10	ND	–	45.2 ± 1.0	2.1	ND	–	45.4 ± 0.5	0.7	0.20

[a] Tartrazine
[b] Sunset yellow
[c] Not detected
[d] Mean of 6 replicates of measurement
[e] Confidence Interval ($\alpha = 0.05, N = 6$)
[f] Mean of 3 replicates of measurement
[g] For seven degrees of freedom at 95 % confidence level, the tabulated t-value is 2.36.

HSI, Grayscale + RGB, Grayscale + HSI, RGB + HSI, and RGB + Grayscale + HSI color models to build the PLS model for the simultaneous determination of Tar and SY.

The results, presented in Table 5, indicate that combination of RGB + Grayscale + HSI color histograms provided the best predictive performance. The RMSECV values were recorded at 0.10 mg/L for Tar and 0.13 mg/L for SY. The R^2_{Pred} values were exceptionally high at 0.9977 and 0.9989 for Tar and SY, respectively.

As shown in Table 5, data combination has enhanced the performance of the multivariate calibration model, underscoring its strong predictive capability (Fig. 3). The improved results due to this solution, color histogram combination, were demonstrated in several studies De Sousa Fernandes et al., 2019; Reile et al., 2020).

The results in Table 6 clearly demonstrate that all PLS models incorporating the color channels (RGB, CMYK, grayscale, HSI), effective color channels (Green, Blue, Yellow, grayscale, Saturation, Intensity), and color histogram combination (RGB+ Grayscale+ HSI) were suitable for simultaneous prediction of Tar and SY, achieving REP values lower than 5 % and R^2_{Pred} values higher than 0.99. As shown, the PLS-assisted RGB+ Grayscale+ HSI histograms achieved the best overall predictive performance (Table 6). From a food analysis perspective, it is essential to develop new methods that ensure both high accuracy and precision. In this study, the PLS-assisted RGB+ Grayscale+ HSI histograms were therefore applied for the quantification of Tar and SY in soft drink samples.

3.3. Real sample analysis

To signify the applicability of the PLS-assisted RGB+ Grayscale +HSI histograms, the simultaneous determination of Tar and SY in 10 soft drink samples was performed and compared with HPLC (Table 7). These real samples were not spiked with analytes, and the concentrations of Tar in the soft drinks were below the LOD determined by scanner -based colorimetry. As a result, Tar could not be detected. The relative standard deviation (RSD) values for six replicate measurements were $\leq$ 2.6 % using the PLS-assisted RGB+ Grayscale+ HSI histograms-based method

Table 8
Simultaneous determination of Tar and SY in a spiked soft drink sample (sample: S1) by PLS-assisted RGB+ Grayscale+ HSI histograms and HPLC.

Tar[a]							
Added (mg/L)	Found (mg/L)		Recovery (%)[b]		RSD (%)		t-test[g]
	PLS	HPLC	PLS	HPLC	PLS	HPLC	
0	ND[c]	ND	—	—	1.5	2.7	—
30	30.5[d] ± 0.5[e]	30.4[f] ± 0.9	101.6	101.5	2.1	2.5	0.04
35	35.5 ± 0.7	35.3 ± 1.0	101.4	100.8	1.4	2.4	0.41
40	39.9 ± 0.6	40.4 ± 1.1	99.7	101.1	1.5	2.7	1.17
			SY[h]				
0	30.3 ± 0.6	30.3 ± 1.1	—	—	2.0	3.7	0.06
20	50.3 ± 1.4	50.6 ± 1.2	99.8	101.6	2.7	2.4	0.49
25	55.6 ± 0.8	55.2 ± 1.9	101.3	99.3	1.4	3.5	0.22
30	60.7 ± 1.3	60.1 ± 1.9	101.3	99.0	2.1	3.2	0.6

[a] Tartrazine
[b] Recovery (%) $= \frac{\text{C found} - \text{Creal}}{\text{C added}} \times 100$
[c] Not detected
[d] Mean of 6 replicates of measurement
[e] Confidence Interval ($\alpha = 0.05$, $N = 6$)
[f] Mean of 3 replicates of measurement;
[g] For Nine degrees of freedom at 95 % confidence level, the tabulated t-value is 2.26
[h] Sunset yellow.

and were not ≥4.6 % for three replicate determinations using the HPLC method.

To validate the accuracy of Tar and SY determination in the soft drink samples, a *t*-test was conducted to compare the results obtained using PLS-assisted RGB + Grayscale + HSI histograms and HPLC. The calculated t-value is presented in Table 7. At the 95 % confidence level, the difference between the results obtained by the two methods was not statistically significant, as the t-value was lower than the critical t-value (Abdelwahed et al., 2024). In summary, it can be concluded that the two methods produce comparable results.

To ensure a more robust evaluation of the proposed method's performance, in addition to the analysis of real samples, Tar and SY were simultaneously determined in a spiked sample (S1) containing known concentrations. To validate the obtained results, Tar and SY in the spiked sample were also analyzed using HPLC, and the recovery results are summarized in Table 8.

The recoveries achieved using the PLS-assisted RGB+ Grayscale+ HSI histograms ranged from 99.7 % to 101.6 %, with a mean recovery of 100.9 % for Tar. For SY, recoveries ranged from 99.9 % to 101.3 %, with a mean recovery of 100.8 %. The HPLC method also demonstrated strong performance, yielding mean recoveries of 101.4 % for Tar and 100.3 % for SY.

To sum up the findings, the satisfactory results obtained using the PLS-assisted RGB+ Grayscale + HSI histograms indicate that this method provides results comparable to those of HPLC. The *t*-test indicates that the results obtained from the developed and standard methods are equivalent (Table 8).

These findings further highlight the proposed method's potential for routine analysis in the beverage industry, demonstrating its reliability for quality control purposes.

The analytical parameters of PLS-assisted RGB + Grayscale+ HSI histograms and several other methods for the determination of Tar and SY were compared in Table 9. The results indicate that this method

Table 9
Comparison of this study with the literature.

Analyte	Real sample	Digital device	Color model	Multivariate calibration method	Linear range (mg/L)	R^2	LOD[c] (mg/L)	RMSECV[d] (mg/L)	RMSEP[e] (mg/L)	REP[f] (%)	Ref.
SY[a]	Orange beverages	Scanner	RGB	PLS	7.8–39.7	0.9702	NR[g]	1.3	1.3	NR	Botelho et al., 2014
SY	Chocolate-orange, Jelly-yellow	Smartphone	RGB	NR	25–500	0.9981	5.28	NR	NR	NR	Saadati, 2021
SY	Chocolated orange, Soft drink orange, Jelly powdered watermelon	Scanner	RGB	NR	30–250	0.9989	7.70	NR	NR	NR	Sorouraddin et al., 2015
Tar[b]	Soda drinks	Smartphone	RGB HSV	PLS	0–20	0.9953	1.2	NR	NR	NR	Jacinto et al., 2023
Tar	Ice-pop, Liquid candy, Liquid sweetener, Liqueur beverage, Food Coloring	Scanner	RGB	PLS	6–40	NR	1.8	3.3	3	NR	Vidal et al., 2018
SY	Soft drinks	Scanner	RGB+ Grayscale + HSI histograms	PLS	2–29	0.9988	0.9	0.13	0.10	1.6	This study
Tar	Soft drinks	Scanner	RGB+ Grayscale + HSI histograms	PLS	3–22	0.9998	0.6	0.10	0.21	1.0	This study

[a] Sunset yellow
[b] Tartrazine
[c] Limit of detection
[d] Root mean square error of cross validation
[e] Root mean square of error prediction
[f] Relative error of prediction
[g] Not reported.

offers significantly better applicability for accurate and precise simultaneous analysis of these analytes in real samples.

4. Conclusion

In this study, digital images captured using a flatbed scanner were transformed into various color models, including RGB, CMYK, and HSI, to serve as multivariate input data for PLS models. The flatbed scanner, an inexpensive and widely accessible tool in most laboratories, offers the advantages of fast image acquisition and user-friendly processing. A significant limitation of colorimetric methods is the lack of specificity validation. Specificity refers to the method's ability to discriminate between the desired analytes and interferences present in real samples. To resolve this limitation, in addition to the analysis of real samples, Tar and SY were simultaneously determined in a spiked sample containing known concentrations of the analytes. The results indicated that PLS models utilizing color channels (RGB, CMYK, grayscale, HSI), effective color channels (Green, Blue, Yellow, Saturation, Intensity), and combined color histograms (RGB + Grayscale + HSI) were suitable for predicting Tar and SY simultaneously. Among these, the PLS-assisted RGB + Grayscale + HSI histograms provided the best overall predictive performance. Satisfactory results were achieved in analyzing Tar and SY in soft drink samples using this approach, yielding outcomes comparable to those obtained with HPLC. However, unlike HPLC, which is time-consuming, costly, and requires solvents and skilled personnel, the proposed method is cost-effective, rapid, and easy to operate and implement. These attributes highlight its potential as a practical alternative for routine analysis of synthetic dyes in beverages.

CRediT authorship contribution statement

Seyyedeh Fatemeh Hosseini: Writing – original draft, Methodology, Formal analysis, Data curation. **Tahereh Heidari:** Supervision. **Ameneh Zendegi-Shiraz:** Validation. **Majid Ameri:** Validation.

Declaration of competing interest

The authors declare that they have no known competing financial interests or personal relationships that could have appeared to influence the work reported in this paper.

Data availability

Data will be made available on request.

Acknowledgment

The authors gratefully acknowledge the financial support of this research by Ferdowsi University of Mashhad (Grant No. 3/57113) for this project.

References

Abdelwahed, F. T., Eltabey, R. M., El-Defrawy, M. M., & Mortada, W. I. (2024). Dispersive liquid–liquid microextraction based on solidification of floating organic droplet and spectrophotometric determination of Allura red using green deep eutectic solvent as disperser solvent: Green profile assessment. *Microchemical Journal, 206*, Article 111432. https://doi.org/10.1016/j.microc.2024.111432

Agbokponto, J. E., Kpaibe, A. P. S., Yemoa, L. A., Assanhou, A. G., Ganfon, H., Gbassi, G. K., & Aké, M. (2022). Simultaneous determination by HPLC-UV vis of Tartrazine and sunset yellow in soft drinks sold in Benin. *American Journal of Analytical Chemistry, 13*(8), 277–288. https://doi.org/10.4236/ajac.2022.138019

Ahmed, W. K. (2013). Advantages and disadvantages of using MATLAB/ode45 for solving differential equations in engineering applications. *International Journal of Engineering, 7*(1), 25–31.

Amchova, P., Siska, F., & Ruda-Kucerova, J. (2024). Safety of tartrazine in the food industry and potential protective factors. *Heliyon, 10*, Article e38111. https://doi.org/10.1016/j.heliyon.2024.e38111

Amsaraj, R., & Mutturi, S. (2021). Real-coded GA coupled to PLS for rapid detection and quantification of tartrazine in tea using FT-IR spectroscopy. *LWT - Food Science and Technology, 139*, Article 110583. https://doi.org/10.1016/j.lwt.2020.110583

Amsaraj, R., & Mutturi, S. (2023). Rapid detection of sunset yellow adulteration in tea powder with variable selection coupled to machine learning tools using spectral data. *Journal of Food Science and Technology, 60*(5), 1530–1540. https://doi.org/10.1007/s13197-023-05694-3

Amsaraj, R., & Mutturi, S. (2024). Classification and quantification of multiple adulterants simultaneously in black tea using spectral data coupled with chemometric analysis. *Journal of Food Composition and Analysis, 125*, Article 105715. https://doi.org/10.1016/j.jfca.2023.105715

Asadollahi, S., Sohrabi, M. R., & Mofavvaz, S. (2022). Rapid simultaneous spectrophotometric determination of food dyes in soft drink using continuous wavelet transform and multivariate calibration methods. *Iranian journal of chemistry and chemical engineering, 41*(5), 1682–1693. https://doi.org/10.30492/ijcce.2021.523573.4543

Bakhnooh, F., & Arvand, M. (2024). A novel photoelectrochemical approach with "signal-off" pattern for anodic detection of sunset yellow in food samples based on Bi2WO6/TiO2 NTAs heterostructure nanocomposite. *Food Chemistry, 438*, Article 138070. https://doi.org/10.1016/j.foodchem.2023.138070

Banc, R., Filip, L., Cozma-Petrut, A., Ciobarca, D., & Miere, D. (2024). Yellow and red synthetic food dyes and potential health hazards: A Mini review. *Bull. University Agriculture Science Vet. Med. Cluj-Napoca Food Science Technology, 81*, 1–17. https://doi.org/10.15835/buasvmcn-fst:2024.0005

Beltrame, K. K., Gonçalves, T. R., Março, P. H., Gomes, S. T. M., Matsushita, M., & Valderrama, P. (2019). Application of digital images and multivariate calibration for the quantification of anthocyanin and antioxidant activity in grape juice. *Australian Journal of Grape and Wine Research, 25*(2), 156–160. https://doi.org/10.1111/ajgw.12387

Botelho, B. G., Dantas, K. C., & Sena, M. M. (2017). Determination of allura red dye in hard candies by using digital images obtained with a mobile phone and N-PLS. *Chemometrics and Intelligent Laboratory Systems, 167*, 44–49. https://doi.org/10.1016/j.chemolab.2017.05.004

Botelho, B. G., de Assis, L. P., & Sena, M. M. (2014). Development and analytical validation of a simple multivariate calibration method using digital scanner images for sunset yellow determination in soft beverages. *Food Chemistry, 159*, 175–180. https://doi.org/10.1016/j.foodchem.2014.03.048

Brereton, R. G. (2003). *Chemometrics: Data analysis for the laboratory and chemical plant*. John Wiley & Sons. https://doi.org/10.1002/0470863242

Brereton, R. G. (2007). *Applied chemometrics for scientists*. John Wiley & Sons. https://doi.org/10.1002/9780470057780

Brereton, R. G. (2018). *Chemometrics: Data driven extraction for science*. John Wiley & Sons. https://doi.org/10.1002/9781118904695

Canero, F. M., Rodriguez-Galiano, V., & Aragones, D. (2024). Machine learning and feature selection for soil spectroscopy. An evaluation of random Forest wrappers to predict soil organic matter, clay, and carbonates. *Heliyon, 10*(9). https://doi.org/10.1016/j.heliyon.2024.e30228

Chaudhari, S. S., Patil, P. O., Bari, S. B., & Khan, Z. G. (2024). A comprehensive exploration of tartrazine detection in food products: Leveraging fluorescence nanomaterials and electrochemical sensors: Recent progress and future trends. *Food Chemistry, 433*, Article 137425. https://doi.org/10.1016/j.foodchem.2023.137425

Choi, M. G., Lee, Y. J., Chang, I. J., Ryu, H., Yoon, S., & Chang, S. K. (2018). Flatbed-scanner-based colorimetric Cu2+ signaling system derived from a coumarin–benzopyrylium conjugated dye. *Sensors and Actuators B: Chemical, 268*, 22–28. https://doi.org/10.1016/j.snb.2018.04.068

Costa, R. A., Morais, C. L., Rosa, T. R., Filgueiras, P. R., Mendonça, M. S., Pereira, I. E., … Romão, W. (2020). Quantification of milk adulterants (starch, H2O2, and NaClO) using colorimetric assays coupled to smartphone image analysis. *Microchemical Journal, 156*, Article 104968. https://doi.org/10.1016/j.microc.2020.104968

Darabi, R., & Shabani-Nooshabadi, M. (2021). NiFe2O4-rGO/ionic liquid modified carbon paste electrode: An amplified electrochemical sensitive sensor for determination of sunset yellow in the presence of Tartrazine and Allura red. *Food Chemistry, 339*, Article 127841. https://doi.org/10.1016/j.foodchem.2020.127841

De Araújo, T. K. L., Nóbrega, R. O., de Sousa Fernandes, D. D., de Araújo, M. C. U., Diniz, P. H. G. D., & da Silva, E. C. (2021). Non-destructive authentication of gourmet ground roasted coffees using NIR spectroscopy and digital images. *Food Chemistry, 364*, Article 130452. https://doi.org/10.1016/j.foodchem.2021.130452

De Morais, C. D. L. M., & de Lima, K. M. G. (2015). Determination and analytical validation of creatinine content in serum using image analysis by multivariate transfer calibration procedures. *Analytical Methods, 7*(16), 6904–6910. https://doi.org/10.1039/c5ay01369k

De Sousa Fernandes, D. D., Romeo, F., Krepper, G., Di Nezio, M. S., Pistonesi, M. F., Centurión, M. E., & Diniz, P. H. G. D. (2019). Quantification and identification of adulteration in the fat content of chicken hamburgers using digital images and chemometric tools. *Lwt, 100*, 20–27. https://doi.org/10.1016/j.lwt.2018.10.034

Diniz, P. H. G. D. (2020). Chemometrics-assisted color histogram-based analytical systems. *Journal of Chemometrics, 34*(12), Article e3242. https://doi.org/10.1002/cem.3242

Do Nascimento, G. E., Cavalcanti, V. O. M., Santana, R. M. R., Sales, D. C. S., Rodríguez-Díaz, J. M., Napoleão, D. C., & Duarte, M. M. M. B. (2020). Degradation of a sunset yellow and tartrazine dye mixture: Optimization using statistical design and empirical mathematical modeling. *Water, Air, & Soil Pollution, 231*, 1–17. https://doi.org/10.1007/s11270-020-04547-5

Dos Santos Pereira, E. V., de Sousa Fernandes, D. D., de Almeida, L. F., Maciel, M. I. S., & Diniz, P. H. G. D. (2022). Goat milk authentication by one-class classification of digital image-based fingerprint signatures: Detection of adulteration with cow milk.

Microchemical Journal, 180, Article 107640. https://doi.org/10.1016/j.microc.2022.107640

EFSA Panel on Food Additives and Nutrient Sources Added to Food. (2009a). Scientific opinion on the re-evaluation of sunset yellow FCF (E 110) as a food additive. *EFSA Journal, 7*(11), 1330. https://doi.org/10.2903/j.efsa.2009.1330

EFSA Panel on Food Additives and Nutrient Sources Added to Food. (2009b). Scientific opinion on the re-evaluation Tartrazine (E 102). *EFSA Journal, 7*(11), 1331. https://doi.org/10.2903/j.efsa.2009.1331

EFSA Panel on Food Additives and Nutrient Sources added to Food (ANS). (2014). Reconsideration of the temporary ADI and refined exposure assessment for sunset yellow FCF (E 110). *EFSA Journal, 12*(7), 3765.

Fan, Y., Zuo, Y., Liu, J., Wang, C., Zhao, X., Ma, J., & Wang, M. (2024). Fabrication of 3D CuFe2O4/Cu0 hierarchical nanostructures on carbon fiber paper by simple hydrothermal method for efficient detection of malachite green, sunset yellow and tartrazine in food samples. *Food Chemistry, 459*, Article 140378. https://doi.org/10.1016/j.foodchem.2024.140378

Fernandes, J. S., de Sousa Fernandes, D. D., Pistonesi, M. F., & Diniz, P. H. G. D. (2023). Tea authentication and determination of chemical constituents using digital image-based fingerprint signatures and chemometrics. *Food Chemistry, 421*, Article 136164. https://doi.org/10.1016/j.foodchem.2023.136164

Fiedoruk-Pogrebniak, M. (2024). Mathematical processing of RGB data in microfluidic paper-based analytical devices. *Scientific Reports, 14*(1), Article 13635. https://doi.org/10.1038/s41598-024-63546-2

Flores-Aguilar, J. F., Medrano, L. C., Perez-Escalante, E., Rodriguez, J. A., Camacho-Mendoza, R. L., & Ibarra, I. S. (2019). Large-volume sample stacking with polarity switching for analysis of azo dyes in water samples by capillary electrophoresis. *International Journal of Environmental Analytical Chemistry, 99*(13), 1255–1267. https://doi.org/10.1080/03067319.2019.1618461

Grudpan, K., Kolev, S. D., Lapanantnopakhun, S., McKelvie, I. D., & Wongwilai, W. (2015). Applications of everyday IT and communications devices in modern analytical chemistry: A review. *Talanta, 136*, 84–94. https://doi.org/10.1016/j.talanta.2014.12.042

Guedes, W. N., & Pereira, F. M. V. (2019). Raw sugarcane classification in the presence of small solid impurity amounts using a simple and effective digital imaging system. *Computers and Electronics in Agriculture, 156*, 307–311. https://doi.org/10.1016/j.compag.2018.11.039

Harris-Love, M. O., Seamon, B. A., Teixeira, C., & Ismail, C. (2016). Ultrasound estimates of muscle quality in older adults: Reliability and comparison of Photoshop and ImageJ for the grayscale analysis of muscle echogenicity. *PeerJ, 4*, Article e1721. https://doi.org/10.7717/peerj.1721

Hua, C., Lyu, L., Ryu, H. S., Park, S. Y., Lim, N. K., Abueva, C., & Chung, P. S. (2020). Design and evaluation of a scalding animal model by the boiling water method. *Medical Lasers; Engineering, Basic Research, and Clinical Application, 9*(1), 51–57. https://doi.org/10.25289/ML.2020.9.1.51

Jacinto, C., Maza Mejía, I., Khan, S., López, R., Sotomayor, M. D., & Picasso, G. (2023). Using a smartphone-based colorimetric device with molecularly imprinted polymer for the quantification of Tartrazine in soda drinks. *Biosensors, 13*(6), 639. https://doi.org/10.3390/bios13060639

Jia, B., Wang, W., Ni, X., Lawrence, K. C., Zhuang, H., Yoon, S. C., & Gao, Z. (2020). Essential processing methods of hyperspectral images of agricultural and food products. *Chemometrics and Intelligent Laboratory Systems, 198*, Article 103936. https://doi.org/10.1016/j.chemolab.2020.103936

Kumar, K. (2021). Partial least square (PLS) analysis: Most favorite tool in chemometrics to build a calibration model. *Resonance, 26*, 429–442. https://doi.org/10.1007/s12045-021-1140-1

Lin, Y., Ma, J., Sun, D. W., Cheng, J. H., & Wang, Q. (2023). A pH-responsive colorimetric sensor array based on machine learning for real-time monitoring of beef freshness. *Food Control, 150*, Article 109729. https://doi.org/10.1016/j.foodcont.2023.109729

Lozano, V. A., de la Peña, A. M., & Escandar, G. M. (2014). A second-order fluorimetric approach based on a boron dipyrromethene tetraamide derivative for hg (II) chemosensing in water and fish samples. *Analytical Methods, 6*(21), 8535–8543. https://doi.org/10.1039/C4AY01757A

Nakanishi, T., Chophuk, P., & Chinnasarn, K. (2024). Evolving feature selection: Synergistic backward and forward deletion method utilizing global feature importance. *IEEE Access*, (99)https://doi.org/10.1109/ACCESS.2024.3418499, 1-1.

Ostad, M. A., & Heidari, T. (2020). Determination and evaluation components affecting the characteristics of synthesized of au nanorods by the UV–vis spectrophotometer, dynamic light scattering, and scanner. *Inorganic and Nano-Metal Chemistry, 51*(3), 374–382. https://doi.org/10.1080/24701556.2020.1790002

Park, J., Cho, Y. S., Seo, D. W., & Choi, J. Y. (2024). An update on the sample preparation and analytical methods for synthetic food colorants in food products. *Food Chemistry, 459*, Article 140333. https://doi.org/10.1016/j.foodchem.2024.140333

Pedjie, N. (2012). *Analysis of color additives in beverages with the PerkinElmer Flexar FX-15 system equipped with a PDA detector*. USA: Application note, PerkinElmer, Waltham. <http://www.perkinelmer.com/CMSResources/Images/44 134896APP_Food_Additives_in_Beverages.Pdf>.

Qashqai, N., & Heidari, T. (2023). A histogram-based technique for simultaneous colorimetric determination of malachite green and brilliant green using Triton X-100 micelle. *Journal of AOAC International, 106*(4), 1098–1108. https://doi.org/10.1093/jaoacint/qsad020

Rahma, R. A., Nugroho, R. A., Kartini, D., Faisal, M. R., & Abadi, F. (2023). Combination of texture feature extraction and forward selection for one-class support vector machine improvement in self-portrait classification. *International Journal of Electrical & Computer Engineering, 13*(1), 2088–8708. https://doi.org/10.11591/ijece.v13i1.pp425-434

Ramo, L. B., Nobrega, R. O., Fernandes, D. D., Lyra, W. S., Diniz, P. H., & Araujo, M. C. (2024). Determination of moisture and total protein and phosphorus contents in powdered chicken egg samples using digital images, NIR spectra, data fusion, and multivariate calibration. *Journal of Food Composition and Analysis, 127*, Article 105940. https://doi.org/10.1016/j.jfca.2023.105940

Reile, C. G., Rodríguez, M. S., de Sousa Fernandes, D. D., de Araújo Gomes, A., Diniz, P. H. G. D., & Di Anibal, C. V. (2020). Qualitative and quantitative analysis based on digital images to determine the adulteration of ketchup samples with Sudan I dye. *Food Chemistry, 328*, Article 127101. https://doi.org/10.1016/j.foodchem.2020.127101

Ribeiro, F. C., Oliveira, A. S., Araújo, A., Marinho, W., Schneider, M. P., Pinto, L., & Gomes, A. A. (2019). Detection oxidative degradation in lubricating oil under storage conditions using digital images and chemometrics. *Microchemical Journal, 147*, 622–627. https://doi.org/10.1016/j.microc.2019.03.087

Riedel, R., Florides, C., Stein, S., Spütz, K., Guerrero, D. A., & Konrad, C. (2023). Improving parameter traceability in model-based product development processes through integration of Python-based domain models. *Procedia CIRP, 119*, 539–544. https://doi.org/10.1016/j.procir.2023.04.009

Rovina, K., Siddiquee, S., & Shaarani, S. M. (2017). A review of extraction and analytical methods for the determination of tartrazine (E 102) in foodstuffs. *Critical Reviews in Analytical Chemistry, 47*(4), 309–324. https://doi.org/10.1080/10408347.2017.1287558

Rozamliana, J., Gurung, J., & Pulikkal, A. K. (2024). Exploring the interactions of anionic dye tartrazine with cationic surfactants in aqueous solution: Insights into micellization and interfacial properties. *Inorganic Chemistry Communications, 159*, Article 111740. https://doi.org/10.1016/j.inoche.2023.111740

Saadati, M. (2021). Smartphone-based digital image analysis for determination of some food dyes in commercial products. *Food Analytical Methods, 14*(11), 2367–2374. https://doi.org/10.1007/s12161-021-02059-4

Santos, V. H. J. M. D., Pontin, D., Oliveira, G. S., Siqueira, T. D. A., & Seferin, M. (2020). Multivariate analysis of digital images as an alternative to monitor dye degradation by the Fenton process. *Química Nova, 43*, 599–606. https://doi.org/10.21577/0100-4042.20170531

Song, W., Song, Z., Vincent, J., Wang, H., & Wang, Z. (2020). Quantification of extra virgin olive oil adulteration using smartphone videos. *Talanta, 216*, Article 120920. https://doi.org/10.1016/j.talanta.2020.120920

Sorouraddin, M. H., Saadati, M., & Mirabi, F. (2015). Simultaneous determination of some common food dyes in commercial products by digital image analysis. *Journal of Food and Drug Analysis, 23*(3), 447–452. https://doi.org/10.1016/j.jfda.2014.10.007

Swain, M. J., & Ballard, D. H. (1991). Color indexing. *International Journal of Computer Vision, 7*(1), 11–32. https://doi.org/10.1007/BF00130487

Taei, M., Salavati, H., Fouladgar, M., & Abbaszadeha, E. (2020). Simultaneous determination of sunset yellow and tartrazine in soft drinks samples using nanocrystallites of spinel ferrite-modified electrode. *Iranian Chemical Communication, 8*(1), 67–79. https://doi.org/10.30473/icc.2019.45932.1543

Timothy, M., & Forlano, P. M. (2019). A versatile macro-based neurohistological image analysis suite for ImageJ focused on automated and standardized user interaction and reproducible data output. *Journal of Neuroscience Methods, 324*, Article 108286. https://doi.org/10.1016/j.jneumeth.2019.04.009

Vidal, M., & Amigo, J. M. (2012). Pre-processing of hyperspectral images. Essential steps before image analysis. *Chemometrics and Intelligent Laboratory Systems, 117*, 138–148.

Vidal, M., Garcia-Arrona, R., Bordagaray, A., Ostra, M., & Albizu, G. (2018). Simultaneous determination of color additives tartrazine and allura red in food products by digital image analysis. *Talanta, 184*, 58–64. https://doi.org/10.1016/j.talanta.2018.02.111

Wang, J., Wu, J., Sun, M., Bai, J., & Bo, X. (2024). Pt nanoparticles/laser-engraved graphene-based integrated electrochemical platform for point-of-use determination of ponceau 4R, amaranth and tartrazine in food. *Food Chemistry, 435*, Article 137611. https://doi.org/10.1016/j.foodchem.2023.137611

Wang, Z., Liang, X., Wu, Z., Lin, J., & Huang, J. (2015). A novel method for measuring anterior segment area of the eye on ultrasound biomicroscopic images using photoshop. *PLoS One, 10*(3), Article e0120843.

Wold, S., Sjöström, M., & Eriksson, L. (2001). PLS-regression: A basic tool of chemometrics. *Chemometrics and Intelligent Laboratory Systems, 58*(2), 109–130. https://doi.org/10.1016/S0169-7439 (01)00155-1

Wu, J. H., & Lee, H. L. (2020). Determination of sunset yellow and tartrazine in drinks using screen-printed carbon electrodes modified with reduced graphene oxide and NiBTC frameworks. *Microchemical Journal, 158*, Article 105133. https://doi.org/10.1016/j.microc.2020.105133

Zhang, H., Low, C. Y., Smoliar, S. W., & Wu, J. H. (1995, January). Video parsing, retrieval and browsing: An integrated and content-based solution. In *Proceedings of the third ACM international conference on multimedia* (pp. 15–24). https://doi.org/10.1145/217279.215068

Zhang, Q., Ao, Y., Liu, J., Tang, S., Tian, F., Tian, X., & Xie, M. (2025). Red-emissive carbon dot as fluorescent probe for the sensitive detection of sunset yellow in foodstuffs. *Food Chemistry, 463*, Article 141477. https://doi.org/10.1016/j.foodchem.2024.141477

Zhang, Y., Li, A., Tian, T., Zhou, X., Liu, Y., Zhao, M., & Zhao, L. (2024). Preparation of amino functionalized magnetic oyster shell powder adsorbent for selective removal of anionic dyes and Pb (II) from wastewater. *International Journal of Biological Macromolecules, 260*, Article 129414. https://doi.org/10.1016/j.ijbiomac.2024.129414